



Usefulness of MRI Scoring System for Differential Diagnosis between Xanthogranulomatous Cholecystitis and Wall-Thickening Type Gallbladder Cancer

황색육아종성 담낭염과 벽비후형 담낭암의 감별진단을 위한 자기공명영상 점수체계의 유용성

Soul Han, MD , Young Hwan Lee, MD* ,
Youe Ree Kim, MD , Eun Gyu Soh, MD 

Department of Radiology, Wonkwang University Hospital, Iksan, Korea

ORCID iDs

Soul Han  <https://orcid.org/0000-0001-5080-8364>
Young Hwan Lee  <https://orcid.org/0000-0001-5893-6571>
Youe Ree Kim  <https://orcid.org/0000-0001-5615-9721>
Eun Gyu Soh  <https://orcid.org/0000-0002-5525-4281>

Purpose To define an MRI scoring system for differentiating xanthogranulomatous cholecystitis (XGC) from wall-thickening type gallbladder cancer (GBC) and compare the diagnostic performance of the scoring system with the visual assessment of radiologists.

Materials and Methods We retrospectively analyzed 23 and 35 patients who underwent abdominal MRI and were pathologically diagnosed with XGC and wall-thickening-type GBC after surgery, respectively. Three radiologists reviewed all MRI findings. We defined a scoring system using these MRI findings for differentiating XGC from wall-thickening type GBC and compared the area under the curve (AUC) of the scoring system with the visual assessment of radiologists.

Results Nine MRI findings showed significant differences in differentiating the two diseases: diffuse gallbladder wall thickening ($p < 0.001$), mucosal uniformity ($p = 0.002$), intramural T2-high signal intensity ($p < 0.001$), mucosal retraction ($p = 0.016$), gallbladder stones ($p < 0.001$), T1-intermediate to high-signal intensity ($p = 0.033$), diffusion restriction ($p = 0.005$), enhancement pattern ($p < 0.001$), and phase of peak enhancement ($p = 0.008$). The MRI scoring system showed excellent diagnostic perfor-

Received April 4, 2023
Revised May 17, 2023
Accepted June 30, 2023

*Corresponding author

Young Hwan Lee, MD
Department of Radiology,
Wonkwang University Hospital,
895 Muwang-ro, Iksan 54538,
Korea.

Tel 82-63-859-1920
Fax 82-63-851-4749
E-mail yjih@wku.ac.kr

This is an Open Access article distributed under the terms of the Creative Commons Attribution Non-Commercial License (<https://creativecommons.org/licenses/by-nc/4.0>) which permits unrestricted non-commercial use, distribution, and reproduction in any medium, provided the original work is properly cited.

mance with an AUC of 0.972, which was significantly higher than the visual assessment of the reviewers.

Conclusion The MRI scoring system showed better diagnostic performance than the visual assessment of radiologists to differentiate XGC from wall-thickening-type GBC.

Index terms Xanthogranulomatous Cholecystitis; Gallbladder Cancer; Differential Diagnosis; Magnetic Resonance Imaging

INTRODUCTION

Xanthogranulomatous cholecystitis (XGC) is a rare type of chronic cholecystitis characterized by destructive inflammation, intramural nodules with infiltration of foamy histiocytes and macrophages, and proliferative fibrosis (1, 2). Clinical manifestations of XGC include right upper abdominal pain, palpable mass, or positive Murphy's sign; however, these findings are nonspecific for the diagnosis of XGC (3-5). In addition, despite its benign character, XGC shows locally aggressive features with various complications, such as perforation, abscess, and fistula formation, and often extends to adjacent organs (3, 6, 7). Owing to these aggressive features, the radiologic features of XGC overlap with wall-thickening type gallbladder cancer (GBC), and the differential diagnosis of the two diseases often remains challenging. Pathological confirmation with surgery should be performed for an accurate diagnosis (8, 9). The treatment for XGC is simple cholecystectomy, whereas GBC may require wider excision and dissection of regional lymph nodes (10). Therefore, exact pre-operative radiologic diagnosis is vital for appropriate surgery planning (5, 11).

Several studies have reported CT findings for the differentiation of XGC from wall-thickening type GBC (9, 10, 12-15). Ito et al. (10) compared the CT findings of 13 patients with XGC and 33 patients with GBC and defined a scoring system based on the CT findings. The area under the curve (AUC) of the receiver operating characteristic (ROC) curve was 0.941, and when three or more out of five findings were presented, the sensitivity was 77%, and the specificity was 94%. Furuta et al. (16) reported MRI findings of XGC for the first time, and, to our knowledge, there are only two reports of MRI findings for differentiating XGC from wall-thickening type GBC (3, 8).

Therefore, this study aimed to evaluate the MRI findings for differentiating XGC from wall-thickening type GBC using 3 Tesla MRI, define an MRI scoring system, and compare the diagnostic performance of this scoring system with the visual assessment of the radiologists.

MATERIALS AND METHODS

PATIENTS

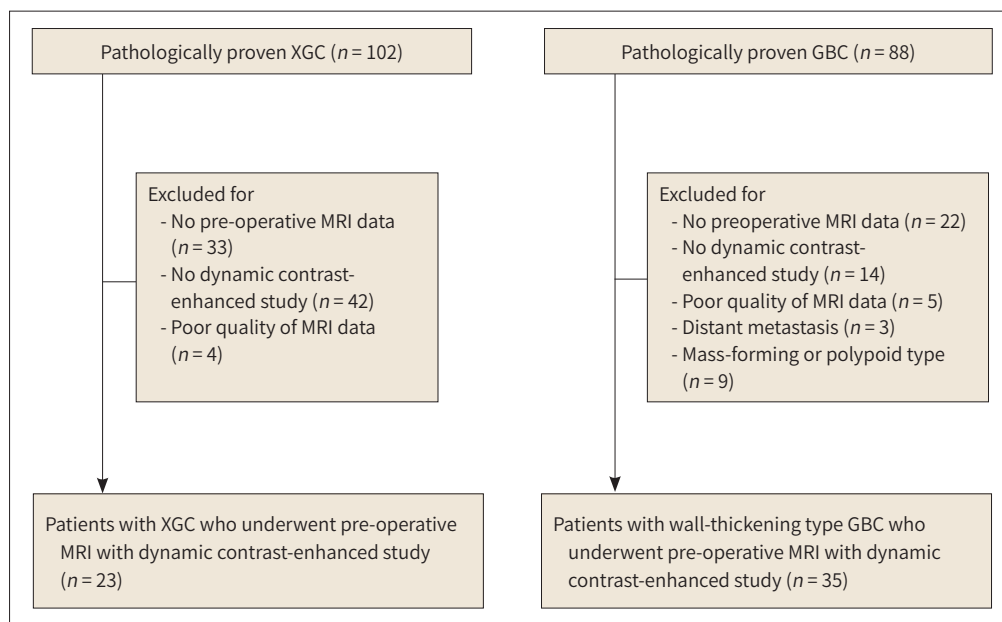
The Institutional Review Board of a tertiary medical hospital (IRB No. 2022-10-018) approved the present study, and the requirement for informed consent was waived. We retrospectively searched our hospital database for patients pathologically confirmed as having XGC or GBC after surgery from January 2011 to August 2021. The database indicated 102 and 88 patients were diagnosed with XGC and GBC, respectively. Among the patients with XGC, 79 were ex-

cluded due to the lack of pre-operative MRI data ($n = 33$), lack of dynamic contrast-enhanced MRI ($n = 42$), and poor quality of MRI ($n = 4$). Among the patients with GBC, 53 were excluded due to the lack of pre-operative MRI data ($n = 22$), lack of dynamic contrast-enhanced MRI ($n = 14$), poor quality MRI imaging ($n = 5$), and distant metastasis ($n = 3$). The GB cancers were classified into mass-forming, polypoid, and wall-thickening types. The mass-forming or polypoid types ($n = 9$) were excluded. Finally, 23 patients with XGC and 35 with wall-thickening type GBC who had undergone at least one pre-operative MRI examination with the dynamic contrast-enhanced study were included in this study (Fig. 1).

MRI PROTOCOL

All MRI studies were performed using 3 Tesla MRI systems (Ingenia CX, Achieva, Philips Healthcare, Best, Netherlands). A 32-channel phased-array receiver coil was used for all MRI sequences. The MRI studies comprised a T1-weighted three-dimensional dual gradient-echo sequence, multi-shot T2-weighted sequence, single-shot T2-weighted sequence, thin-slice T2 half-Fourier acquisition single-shot turbo spin-echo (HASTE) sequence, and thick-slab rapid acquisition relaxation enhancement (RARE) sequence. For the dynamic contrast-enhanced MRI study, the unenhanced, arterial phase (20–30 s), portal phase (60 s), delayed phase (120 s), and hepatobiliary phase (10 min, 20 min) were obtained using a T1-weighted dual-echo multi-point DIXON sequence or a T1-weighted three-dimensional gradient-echo sequence (T1 high-resolution isotropic volume examination, THRIVE, Philips Healthcare) with a spectral attenuated inversion recovery fat suppression technique. For the contrast agent, gadoteric acid (Primovist; Bayer Schering Pharma, Berlin, Germany) was injected intravenously at a rate of 1.5 mL/s and a dose of 0.1 mL/kg, followed by a flush with 20 mL of saline. Diffusion-weighted images (DWI) were obtained using single-shot echo planar imaging with b-values

Fig. 1. Flow chart of patient selection.



GBC = gallbladder cancer, XGC = xanthogranulomatous cholecystitis

of 0, 50, 400, and 800 s/mm². The apparent diffusion coefficient (ADC) was calculated using a mono-exponential function with b-values of 0 and 800 s/mm². Detailed MRI sequence parameters are listed in Table 1.

MRI ANALYSIS

Three radiologists (two board-certified radiologists with 20 and 6 years of experience in interpreting abdominal imaging and a third-year radiologic resident) reviewed all MRI studies of both groups. The reviewers were blinded to the clinical and pathological information of patients. Each reviewer independently made an imaging diagnosis respectively and analyzed the MRI findings in terms of morphologic features, enhancement pattern, and diffusion restriction of the lesion. The final decision on each finding was made by consensus. The analyzed MRI findings were selected based on previous CT or MRI studies (3, 8, 10, 12, 13).

On pre-contrast MRI, the following imaging findings were evaluated by the reviewers: 1) diffuse gallbladder wall thickening, 2) mucosal uniformity, 3) continuity of mucosal line, 4) maximal thickness of gallbladder wall, 5) intramural T2-high signal intensity, 6) gallbladder mucosal retraction, 7) gallbladder stone, 8) extrahepatic bile duct dilatation (> 10 mm or < 10 mm), 9) intrahepatic bile duct dilatation, 10) T1- and T2-signal intensity, 11) presence of chemical shift, 12) presence of liver invasion, and 13) pericholecystic infiltration. The morphologic features of the lesion and the maximal thickness of the gallbladder wall were assessed on a T2-weighted image. The diffuse gallbladder wall thickening was defined that the lesion involving more than two parts of the gallbladder or is more than 3 cm in size at the axial or coronal plane MR image. The T1- and T2-signal intensities of the lesions were evaluated as high-, intermediate-, or low-signal intensity by comparison with the surrounding hepatic parenchyma.

Diffusion restriction was defined as high-signal intensity on DWI with a b-value of 800 s/mm² and combined low signal intensity on the correlated ADC map compared to the surrounding hepatic parenchyma.

The following two findings were evaluated on dynamic contrast-enhanced MRI: 1) enhancement pattern and 2) phase of peak enhancement. We referred to a previously published report by Lee et al. (3) for the enhancement pattern. The enhancement pattern was classified into three types: type 1 pattern was a heterogeneous and thick enhancement of the gallbladder wall; type 2 pattern was well enhancing thick inner layer with a mildly enhanc-

Table 1. MRI Sequences and Parameters

Sequence	TR/TE (ms)	Flip Angle (°)	Section Thickness (mm)	Matrix Size	Bandwidth (Hz/Pixel)	Field of View (cm)
T1-weighted dual GRE	10/2.3	15	6	264 × 264	433	330 × 330
Breath-hold multi-shot T2-weighted imaging	1160/80	90	6	300 × 211	486	330 × 330
Single-shot T2-weighted imaging	2300/79	90	6	256 × 256	1688	330 × 330
Thick-slab RARE	6300/920	90	40	252 × 252	417	250 × 250
Thin-slice T2 HASTE	720/80	90	3	232 × 210	653	268 × 268
DWI/ADC	1380/56	90	5	112 × 108	3529	330 × 330
Dynamic study	3.1/1.5	10	5	276 × 170	721	330 × 330

ADC = apparent diffusion coefficient, DWI = diffusion-weighted imaging, GRE = gradient echo, HASTE = half fourier single-shot turbo spine-echo, RARE = rapid acquisition and relaxation enhancement, TE = echo time, TR = repetition time

ing thin outer layer; all other patterns were classified as type 3, including mild and thin enhancement of the inner layer (Fig. 2). For the phase of peak enhancement, the gallbladder wall was assessed according to the priority of enhancement on dynamic MRI examination as the arterial, portal, or delayed phase. When no meaningful enhancement or hyperintensity of the lesion was noted compared to the surrounding hepatic parenchyma on dynamic contrast-enhanced MRI, it was evaluated as a poor enhancement.

DEVELOPMENT OF MRI SCORING SYSTEM

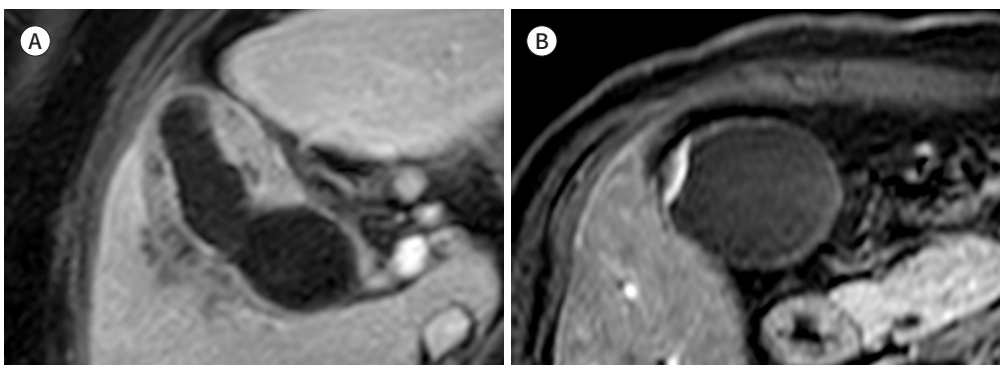
For differentiating XGC from wall-thickening type GBC, we defined a scoring system evaluating the number of findings reflecting XGC among the significant MRI findings. If the finding was observed more frequently in the XGC group, it was scored 1. In contrast, if the finding was observed more frequently in the GBC group, it was scored 0. Findings with more than three categories were also scored as 1 or 0 according to the frequency of each finding. The diagnostic performance of the scoring system was evaluated using the AUC of the ROC curve, and the Youden index was used to determine the optimal cutoff value.

STATISTICAL ANALYSIS

For continuous variables, means, standard deviations, and ranges were presented, and for categorical variables, proportions were presented. The independent *t*-test or Mann-Whitney test was used for the difference in proportions of continuous variables. The Mann-Whitney test was applied when the variables did not follow a normal distribution on the Shapiro-Wilk test. The chi-square or Fisher's exact test was used to analyze proportional differences in categorical variables. Fisher's exact test was applied when the chi-square test was not suitable due to the inadequately small sample size. The AUC of the ROC curve was used to assess and compare the diagnostic performance of our MRI scoring system and the visual assessment of the reviewers. The AUC of each reviewer and scoring system were compared by the method of Hanley & Mcneil. A *p*-value of < 0.05 was considered statistically significant. Statistical analyses were performed using SPSS (version 26, IBM Corp., Armonk, NY, USA) and MedCalc Statistical (version 14.8.1, MedCalc Software Ltd, Ostend, Belgium) software.

Fig. 2. Enhancement patterns on dynamic contrast-enhanced MRI.

A, B. Type 1 pattern (A) is heterogeneous and has thick enhancement of the gallbladder wall; type 2 pattern (B) is well enhancing thick inner layer with a mildly enhancing thin outer layer; all other patterns were classified as type 3.



RESULTS

PATIENT CHARACTERISTICS

The 23 patients with XGC included 12 male and 11 female (mean age, 68 ± 10 years), whereas the 35 patients with GBC included 15 male and 20 female (mean age, 74 ± 8 years). The mean age was significantly higher in the GBC group. Examining pre-operative tumor markers, such as carcinoembryonic antigen (CEA) and carbohydrate antigen 19-9 (CA19-9), was performed on 17 of 23 patients in the XGC group and 29 of 35 in the GBC group. The CEA was higher in the GBC group, but no difference was observed for CA19-9 between the two groups. A description of the patient characteristics is provided in Table 2.

ANALYSIS OF MRI FINDINGS

PRE-CONTRAST MRI

Diffuse gallbladder wall thickening was observed in 20 patients (87%) with XGC and 6 patients (17%) with GBC ($p < 0.001$). Mucosal uniformity was observed in 12 patients (52%) with XGC and 5 patients (14%) with GBC ($p = 0.002$). Intramural T2-high signal intensity was observed in 16 patients (70%) with XGC and 6 patients (17%) with GBC ($p = 0.001$). The gallbladder mucosal retraction was observed in 2 patients (9%) with XGC and 13 patients (37%) with GBC ($p = 0.016$). Gallbladder stones were observed in 20 patients (87%) with XGC and 12 patients (34%) with GBC ($p < 0.001$). Intermediate to high signal intensity on T1-weighted image was observed in 13 patients (57%) with XGC and 10 patients (29%) with GBC ($p = 0.033$). No significant differences were observed between the two groups in the continuity of the mucosal line, the maximal thickness of the gallbladder wall, extrahepatic bile duct dilatation, in-

Table 2. Patient Characteristics of Both Groups

Clinical Characteristics	XGC (n = 23)	Wall-Thickening Type GBC (n = 35)	p-Value
Age (years) *	68 ± 10 (42–82)	74 ± 8 (57–90)	0.004
Male (n) †	12 (52)	15 (43)	0.487
CEA (ng/mL) ‡	2.1 ± 1.7 (0.7–8.1)	224.6 ± 1153.1 (1.2–6218.0)	0.005
CA19-9 (U/mL) ‡	117.3 ± 221.1 (0.8–841.1)	1627.8 ± 4899.9 (0.8–24604.0)	0.090
Pathologic stage §			
		T1bN0	3 (9)
		T2N0	21 (60)
		T2N1	3 (9)
		T3N0	2 (6)
		T3N1	3 (9)
		T3N2	3 (9)

Values are given as mean \pm standard deviation (range) or n (%).

*Independent *t*-test was used.

† Chi-square test was used.

‡ Mann-Whitney U test was used.

§ Pathologic stage was evaluated using American Joint Committee on Cancer guideline 7th or 8th editions. CA19-9 = carbohydrate antigen, CEA = carcinoembryonic antigen, GBC = gallbladder cancer, XGC = xanthogranulomatous cholecystitis

trahepatic bile duct dilatation, T2-signal intensity, presence of chemical shift, presence of liver invasion, and pericholecystic infiltration. The MRI findings are summarized in Table 3.

DIFFUSION-WEIGHTED MRI

Thirty-one patients (89%) with wall-thickening type GBC showed definite diffusion restriction compared to 13 patients (57%) with XGC ($p = 0.005$).

Table 3. MRI Findings of XGC and Wall-Thickening Type GBC

MRI Findings	XGC (n = 23)	Wall-Thickening Type GBC (n = 35)	p-Value	Odds Ratio	95% CI
Pre-contrast MRI					
Diffuse gallbladder wall thickening*	20 (87)	6 (17)	< 0.001	32.222	7.201–144.182
Mucosal uniformity*	12 (52)	5 (14)	0.002	6.545	1.873–22.875
Continuity of mucosal line*	7 (30)	7 (20)	0.364	1.750	0.520–5.895
Maximal thickness of gallbladder wall (mm) [†]	8.7 ± 3.7	9.1 ± 4.4	0.817		
Intramural T2-high signal intensity*	16 (70)	6 (17)	< 0.001	11.048	3.166–38.546
Gallbladder mucosal retraction*	2 (9)	13 (37)	0.016	6.205	1.247–30.864
Gallbladder stone*	20 (87)	12 (34)	< 0.001	12.778	3.151–51.811
Extra-hepatic bile duct dilatation (> 10 mm)*	8 (35)	6 (17)	0.125	2.578	0.755–8.805
Intra-hepatic bile duct dilatation [‡]	5 (22)	4 (11)	0.460	2.153	0.511–9.062
T2-signal intensity [‡]			0.617	1.678	0.564–4.994
Low to intermediate	10 (43)	11 (31)			
High	13 (57)	24 (69)			
T1-signal intensity*			0.033	3.250	1.078–9.797
Low	10 (43)	25 (71)			
Intermediate to high	13 (57)	10 (29)			
Presence of chemical shift [‡]	3 (13)	2 (6)	0.376	2.475	0.380–16.114
Presence of liver invasion*	8 (35)	11 (31)	0.790	1.164	0.381–3.552
Pericholecystic infiltration [‡]	3 (13)	7 (20)	0.725	0.600	0.138–2.607
DWI					
Diffusion restriction*	13 (56)	31 (89)	0.005	5.962	1.580–22.499
Dynamic contrast enhanced MRI					
Enhancement pattern [‡]			< 0.001		
Type 1	13 (57)	7 (20)			
Type 2	3 (13)	24 (69)			
Type 3	7 (30)	4 (11)			
Phase of peak enhancement [‡]			0.008		
Arterial	5 (22)	19 (54)			
Portal	7 (30)	1 (3)			
Delayed	9 (39)	10 (29)			
Poor enhancement	2 (9)	5 (14)			

Values are given as mean ± standard deviation (range) or n (%).

*Chi-square test was used.

[†]Mann-Whitney U test was used.

[‡]Fisher's exact test was used.

CI = confidence interval, DWI = diffusion-weighted image, GBC = gallbladder cancer, XGC = xanthogranulomatous cholecystitis

DYNAMIC CONTRAST-ENHANCED MRI

In the case of the enhancement pattern, more than half (13 patients, 57%) of the patients with XGC showed a type I pattern. In contrast, more than two-thirds (24 patients, 69%) of patients with GBC showed a type II pattern ($p < 0.001$). In the XGC group, peak enhancement of the lesion was noted most commonly in the delayed phase (9 patients, 39%), followed by the portal phase (7 patients, 30%). Conversely, more than half (19 patients, 54%) of the lesions showed peak enhancement in the arterial phase in the GBC group ($p = 0.008$).

MRI SCORING SYSTEM

We defined a scoring system using the nine significant MRI findings for differentiating XGC from wall-thickening-type GBC. Considering the previous results, type I or III was scored as 1 for the enhancement pattern, and type II was scored as 0. If the lesion showed peak enhancement on the portal or delayed phase on dynamic contrast-enhanced MRI, it was scored as 1, and if the lesion showed peak enhancement on the arterial phase or poor enhancement, it was scored as 0. The AUC was 0.972. According to the Youden index, the optimal cutoff value was 5, and the sensitivity, specificity, and accuracy for XGC were 87% (95% confidence interval [CI] = 66–97), 91% (95% CI = 77–98), and 90% (95% CI = 79–96), respectively (Fig. 3). Representative cases of the MRI scoring system in XGC (Fig. 4) and wall-thickening-type GBC (Fig. 5) are shown.

COMPARISON OF DIAGNOSTIC PERFORMANCE OF THE MRI SCORING SYSTEM AND THE VISUAL ASSESSMENT

The sensitivity and specificity were 82% (95% CI = 60–95) and 94% (95% CI = 81–99) for reviewer 1, 91% (95% CI = 71–99), and 86% (95% CI = 70–95) for reviewer 2 and 86% (95% CI = 65–97), and 80% (95% CI = 63–92) for reviewer 3. The AUC was 0.884 for reviewer 1, 0.885 for reviewer 2, and 0.835 for reviewer 3 (Table 4, Fig. 6). The AUC of the scoring system was signif-

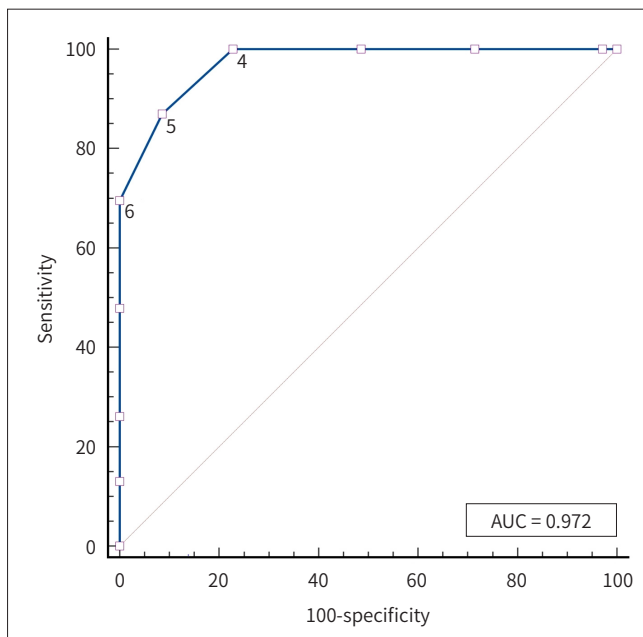


Fig. 3. Receiver operating characteristic curve of the MRI scoring system. The optimal cutoff value is 5, and the sensitivity, specificity and accuracy for xanthogranulomatous cholecystitis are 87% (95% CI = 66–97), 91% (95% CI = 77–98) and 90% (95% CI = 79–96), respectively. AUC = area under the curve, CI = confidence interval

Fig. 4. MRI findings of xanthogranulomatous cholecystitis in an 81-year-old female.

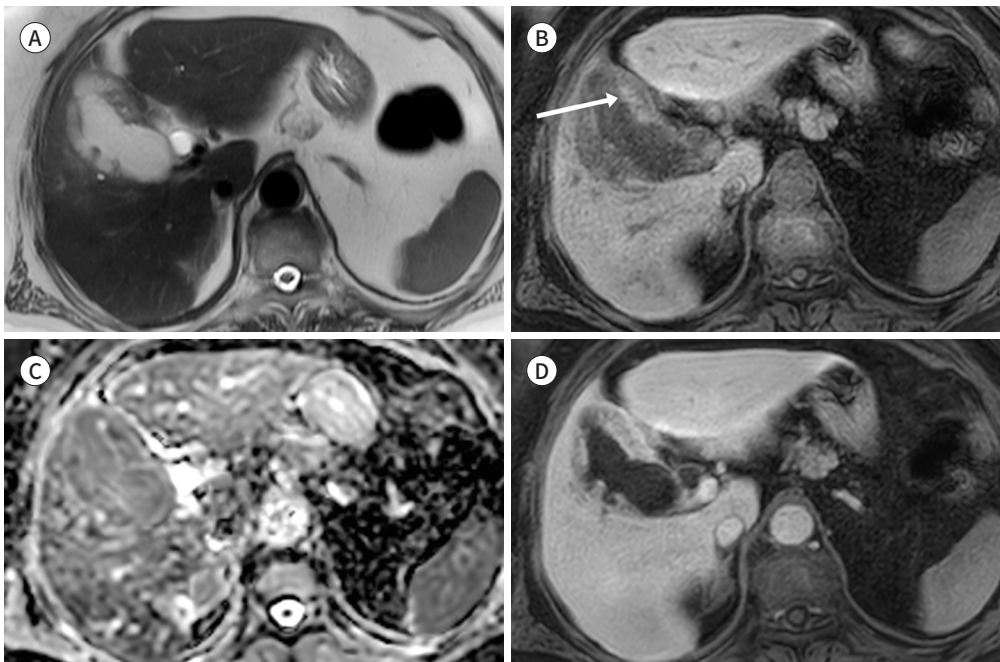
A. T2-weighted image shows diffuse and uniform gallbladder wall thickening with multiple intramural hyperintense nodules. The mucosal retraction is not noted.

B. On fat-saturated T1-weighted image, the thickened gallbladder wall shows intermediate-signal intensity compared to hepatic parenchyma (arrow).

C. On the apparent diffusion coefficient map calculated using a b-value of 0 and 800 s/mm², the thickened gallbladder wall shows intermediate-signal intensity compared with surrounding hepatic parenchyma, indicating no definite diffusion restriction.

D. In the delayed phase of the dynamic MRI study, the gallbladder wall shows thick and heterogeneous enhancement but with lower signal intensity than hepatic parenchyma.

When the MRI scoring system was applied, the score of the lesion was 8 (diffuse gallbladder wall thickening, mucosal uniformity, intramural T2-hyper-intensity, absence of mucosal retraction, gallbladder stone, T1-intermediate to high-signal intensity, absence of diffusion restriction, and enhancement pattern), indicating xanthogranulomatous cholecystitis.



icantly higher than that of the visual assessments of all reviewers ($p = 0.029, 0.032, \text{ and } 0.006$, respectively).

DISCUSSION

In this study, nine significant MRI findings for differentiating XGC from wall-thickening type GBC were identified: diffuse gallbladder wall thickening, mucosal uniformity, intramural T2-high signal intensity, absence of mucosal retraction, gallbladder stone, T1-intermediate to high-signal intensity, diffusion restriction, enhancement pattern, and the phase of peak enhancement. The MRI scoring system showed excellent diagnostic performance with an AUC of 0.972. When the cutoff value was 5, the sensitivity and specificity of the scoring system were high (87%, and 91%, respectively). When the cutoff value was lowered to 4, the sensitivity increased to 100%, and when raised to 6, the specificity increased to 100%. The AUC of the scoring system was significantly higher than the AUC of the visual assessments of

Fig. 5. MRI findings of wall-thickening type gallbladder cancer in an 80-year-old female.

A, B. T2-weighted image showing diffuse thickening of gallbladder wall without mucosal uniformity. The lesion contains multiple T2-hyperintense intramural nodules and shows mucosal retraction (arrow).

C. On the apparent diffusion coefficient map calculated using a b-value of 0 and 800 s/mm², the thickened gallbladder wall shows low-signal intensity compared with adjacent hepatic parenchyma, indicating diffusion restriction.

D. The peak enhancement of the thickened gallbladder wall is shown in the delayed phase of the dynamic MRI study. The lesion shows heterogeneous enhancement.

When the MRI scoring system was applied, the lesion score was 3 (diffuse gallbladder wall thickening, intramural T2-hyperintensity, enhancement pattern, and phase of peak enhancement), indicating a wall thickening-type gallbladder cancer.

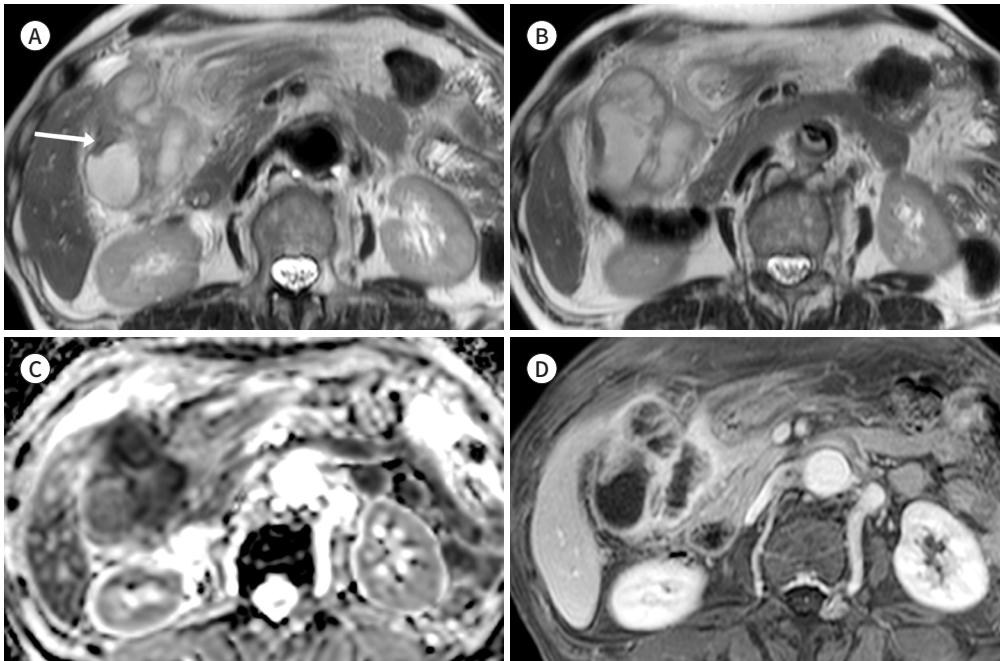


Table 4. Diagnostic Performance of the Visual Assessment and MRI Scoring System

Diagnostic Performance	Sensitivity	Specificity	Accuracy	AUC or the ROC Curves
Reviewer 1	82	94	89	0.884
Reviewer 2	91	86	88	0.885
Reviewer 3	87	80	82	0.835

Values are given as %.

AUC = area under the curve, ROC = receiver operating characteristic

the reviewers. The MRI scoring system can offer objectivity, reliability, and additional diagnostic accuracy. Because of the rarity of the XGC, the MRI scoring system can be more useful for inexperienced readers, such as radiologic residents or clinicians.

The MRI scoring system has no weight set for each MRI finding. The MRI scoring system includes nine parameters, which are too many to apply even the weights in clinical situations. Therefore, a simplified method of counting the observed MRI findings was used.

In previous studies, diffuse gallbladder wall thickening, mucosal uniformity, intramural T2-high signal intensity, gallbladder stones, and diffusion restriction were significantly different for differentiating XGC from wall-thickening-type GBC on ultrasound, CT, or MRI (3, 8,

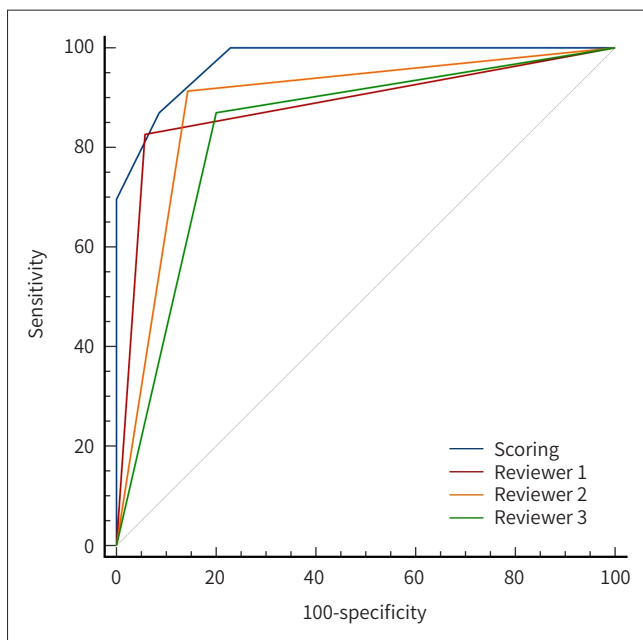


Fig. 6. ROC curves of the MRI scoring system and visual assessment of radiologists.

The area under each ROC curve is 0.884 for reviewer 1, 0.885 for reviewer 2, and 0.835 for reviewer 3. The area under the curve of the scoring system is significantly higher than that of the visual assessments of all reviewers ($p = 0.029, 0.032, \text{ and } 0.006$, respectively). ROC = receiver operating characteristic

10, 12, 13). These findings were also significant in the present study. Although the pathogenesis of XGC is largely unknown, gallbladder stone is considered to be profoundly associated with XGC. The gallbladder stone causes obstruction, increased intraluminal pressure of the gallbladder and rupture of the Rokitansky-Aschoff sinus, and eventually develops into XGC. The inflammatory change of XGC appears in the Rokitansky-Ashoff sinuses, not in the mucosa, resulting in full-thickness involvement of the gallbladder wall. Therefore, the XGC shows diffuse gallbladder wall thickening and mucosal uniformity (3). Histologically, XGC shows intramural nodules representing abscesses and xanthogranulomas, which appear as intramural T2-high signal intensity (12).

The wall-thickening type GBC showed earlier peak enhancement than XGC in a dynamic contrast-enhanced study, similar to the report of Kang et al. (8). This is because malignant tumour growth is accompanied by angiogenesis, while inflammation increases blood flow without angiogenesis (8, 13). For the enhancement pattern, XGC most commonly showed heterogeneous and thick enhancement and wall-thickening type GBC most commonly showed a double layer with well enhancing, thick inner layer, similar to the previous report of Lee et al. (3) GBC originates in the mucosal layer and sequentially invades the outer layer. Therefore, GBC can show a double-layer pattern with well enhancing inner layer and a poorly enhancing outer layer. On the other hand, XGC shows chronic inflammation of full-thickness of the gallbladder wall and heterogeneous single-layer pattern.

There was a case report in which XGC was diagnosed by identifying fat content with the accumulation of intramural foamy histiocytes using the chemical shift phenomenon that shows higher-signal intensity on in-phase images than out-of-phase images (17). However, in this study, the chemical shift phenomenon of the lesion was observed in only five patients (8%) in the XGC group; therefore, it could not be considered an indication of intramural fat content. In contrast, intermediate- to high-signal intensity of the lesion on the T1-weighted image was

observed in 37 patients (57%) in the XGC group, which was significantly different from the GBC group. This finding was also presumed to be owing to the accumulation of foamy histiocytes, and T1-signal intensity was expected to assist in differentiating XGC from wall-thickening type GBC rather than the chemical shift phenomenon. However, the evaluation of T1-signal intensity can be inappropriate owing to the deposition of materials such as fat or iron in the hepatic parenchyma.

Gallbladder mucosal retraction was observed in 14 patients (29%) with wall-thickening type GBC. To our knowledge, this is the first report of gallbladder mucosal retraction. About 20% of intrahepatic cholangiocarcinoma show adjacent hepatic capsular retraction (18), and lung and breast cancers show retraction of adjacent normal tissue or architectural distortion (19, 20); these are owing to the prominent fibrous stroma of malignant neoplasms (18). GBC originates from the mucosal layer, and fibrosis of the neoplasm retracts the adjacent gallbladder wall; therefore, it is presented as a mucosal retraction. XGC is also accompanied by proliferative fibrosis but is involved in full-thickness; hence, it is presumed not to represent mucosal retraction. In the present study, only 6 cases (9%) of XGC showed mucosal retraction, and there was a significant difference between the two groups.

Ito et al. (10) analyzed the CT findings of 13 patients with XGC and 33 patients with GBC for discrimination of the two diseases and defined a scoring system using five CT findings. The AUC of the CT scoring system was 0.941, and then with a score of 3 or more out of 5, a sensitivity of 77% (95% CI = 57–87), and a specificity of 94% (95% CI = 86–98). Compared to the MRI scoring system in our study, the CT scoring system showed a little lower AUC, lower sensitivity, and higher specificity. However, because this study included a very small number of patients with XGC and did not exclude mass-forming type GBC that was easy to discriminate from XGC, the diagnostic performance of the MRI scoring system was presumed to be higher than that of the CT scoring system. In a previous study, MRI showed a higher diagnostic performance than CT in differentiating between the two diseases (3). MRI shows good contrast resolution, and DWI and dynamic contrast-enhanced MRI seem to provide additional diagnostic value. It has been proven that DWI in addition to pre-contrast MRI could improve the discrimination between the two diseases (8).

Our study had several limitations. First, this study was retrospectively designed at a single medical center and may have inherent selective bias. Second, a small number of patients was included in this study. Third, there was no step for validating the MRI scoring system in another independent cohort. Finally, MRI findings were scored as 1 or 0 in the scoring system, although they may have different statistical significances. Therefore, if, in further studies, the scoring system is more delicately designed using multiple grades and weights according to statistical values, better diagnostic performance can be expected.

In conclusion, the scoring system using nine useful MRI findings of morphologic features, enhancement pattern, and diffusion restriction showed better diagnostic performance to differentiate XGC from wall-thickening-type GBC than the visual assessment. The MRI scoring system can provide objectivity, reliability and additional diagnostic value.

Author Contributions

Conceptualization, L.Y.H.; data curation, H.S., S.E.G.; formal analysis, H.S.; investigation, L.Y.H.;

methodology, H.S., L.Y.H., K.Y.R.; project administration, L.Y.H.; software, H.S., K.Y.R., S.E.G.; supervision, L.Y.H.; validation, L.Y.H., K.Y.R., S.E.G.; visualization, H.S.; writing—original draft, H.S.; and writing—review & editing, L.Y.H., K.Y.R., S.E.G.

Conflicts of Interest

The authors have no potential conflicts of interest to disclose.

Funding

This research was supported by Wonkwang University in 2023.

REFERENCES

1. Srinivas GN, Sinha S, Ryley N, Houghton PW. Perfidious gallbladders - a diagnostic dilemma with xantho-granulomatous cholecystitis. *Ann R Coll Surg Engl* 2007;89:168-172
2. Rammohan A, Cherukuri SD, Sathyanesan J, Palaniappan R, Govindan M. Xanthogranulomatous cholecys-titis masquerading as gallbladder cancer: can it be diagnosed preoperatively? *Gastroenterol Res Pract* 2014;2014:253645
3. Lee ES, Kim JH, Joo I, Lee JY, Han JK, Choi BI. Xanthogranulomatous cholecystitis: diagnostic performance of US, CT, and MRI for differentiation from gallbladder carcinoma. *Abdom Imaging* 2015;40:2281-2292
4. Makino I, Yamaguchi T, Sato N, Yasui T, Kita I. Xanthogranulomatous cholecystitis mimicking gallbladder carcinoma with a false-positive result on fluorodeoxyglucose PET. *World J Gastroenterol* 2009;15:3691-3693
5. Khan MR, Begum S. Extended resection for xanthogranulomatous cholecystitis mimicking gallbladder car-cinoma: cases and review of diagnostic approach. *J Pak Med Assoc* 2019;69:256-260
6. Singh VP, Rajesh S, Bihari C, Desai SN, Pargewar SS, Arora A. Xanthogranulomatous cholecystitis: what ev-ery radiologist should know. *World J Radiol* 2016;8:183-191
7. Tongdee R, Maroongroge P, Suthikeree W. The value of MDCT scans in differentiation between benign and malignant gallbladder wall thickening. *J Med Assoc Thai* 2011;94:592-600
8. Kang TW, Kim SH, Park HJ, Lim S, Jang KM, Choi D, et al. Differentiating xanthogranulomatous cholecys-titis from wall-thickening type of gallbladder cancer: added value of diffusion-weighted MRI. *Clin Radiol* 2013;68:992-1001
9. Uchiyama K, Ozawa S, Ueno M, Hayami S, Hirono S, Ina S, et al. Xanthogranulomatous cholecystitis: the use of preoperative CT findings to differentiate it from gallbladder carcinoma. *J Hepatobiliary Pancreat Surg* 2009;16:333-338
10. Ito R, Kobayashi T, Ogasawara G, Kono Y, Mori K, Kawasaki S. A scoring system based on computed tomography for the correct diagnosis of xanthogranulomatous cholecystitis. *Acta Radiol Open* 2020;9:2058460120918237
11. Yabanoglu H, Aydogan C, Karakayali F, Moray G, Haberal M. Diagnosis and treatment of xanthogranuloma-tous cholecystitis. *Eur Rev Med Pharmacol Sci* 2014;18:1170-1175
12. Goshima S, Chang S, Wang JH, Kanematsu M, Bae KT, Federle MP. Xanthogranulomatous cholecystitis: di-agnostic performance of CT to differentiate from gallbladder cancer. *Eur J Radiol* 2010;74:e79-e83
13. Chang BJ, Kim SH, Park HY, Lim SW, Kim J, Lee KH, et al. Distinguishing xanthogranulomatous cholecystitis from the wall-thickening type of early-stage gallbladder cancer. *Gut Liver* 2010;4:518-523
14. Shetty GS, Abbey P, Prabhu SM, Narula MK, Anand R. Xanthogranulomatous cholecystitis: sonographic and CT features and differentiation from gallbladder carcinoma: a pictorial essay. *Jpn J Radiol* 2012;30:480-485
15. Chun KA, Ha HK, Yu ES, Shinn KS, Kim KW, Lee DH, et al. Xanthogranulomatous cholecystitis: CT features with emphasis on differentiation from gallbladder carcinoma. *Radiology* 1997;203:93-97
16. Furuta A, Ishibashi T, Takahashi S, Sakamoto K. MR imaging of xanthogranulomatous cholecystitis. *Radiat Med* 1996;14:315-319
17. Hatakenaka M, Adachi T, Matsuyama A, Mori M, Yoshikawa Y. Xanthogranulomatous cholecystitis: impor-tance of chemical-shift gradient-echo MR imaging. *Eur Radiol* 2003;13:2233-2235
18. Da Ines D, Mons A, Braidy C, Montoriol PF, Garcier JM, Vilgrain V. Hepatic capsular retraction: spectrum of diagnosis at MRI. *Acta Radiol Short Rep* 2014;3:2047981614545667

19. Hsu JS, Han IT, Tsai TH, Lin SF, Jaw TS, Liu GC, et al. Pleural tags on CT scans to predict visceral pleural invasion of non-small cell lung cancer that does not abut the pleura. *Radiology* 2016;279:590-596
20. Shaheen R, Schimmelpenninck CA, Stoddart L, Raymond H, Slanetz PJ. Spectrum of diseases presenting as architectural distortion on mammography: multimodality radiologic imaging with pathologic correlation. *Semin Ultrasound CT MR* 2011;32:351-362

황색육아종성 담낭염과 벽비후형 담낭암의 감별진단을 위한 자기공명영상 점수체계의 유용성

한 솔 · 이영환* · 김유리 · 소은규

목적 황색육아종성 담낭염을 벽비후형 담낭암으로부터 감별진단하기 위한 자기공명영상 (MRI) 점수체계를 고안하고, 그 점수체계의 진단능을 영상의학과 의사의 시각적 평가와 비교하고자 한다.

대상과 방법 복부 MRI 및 수술을 시행한 각각 황색육아종성 담낭염과 벽비후형 담낭암으로 진단된 23명과 35명의 환자를 후향적으로 분석하였다. 세 명의 영상의학과 의사가 모든 MRI 소견을 분석하였다. 저자들은 이러한 MRI 소견을 이용하여 벽비후형 담낭암으로부터 황색육아종성 담낭염을 감별진단하기 위한 점수체계를 고안하였고 이 점수체계의 진단능을 수신자 운영 특성 곡선의 곡선 하 면적을 영상의학과 의사의 시각적 평가와 비교하였다.

결과 9가지의 MRI 소견이 두 질환의 감별에 유의미한 차이를 보였다: 미만형 벽 비후($p < 0.001$), 점막 균일성($p = 0.002$), 벽내 T2 고신호강도($p < 0.001$), 점막 당김($p = 0.016$), 담낭 결석($p < 0.001$), T1 중등도 혹은 고신호강도($p = 0.033$), 확산 제한($p = 0.005$), 조영증강 패턴($p < 0.001$), 조영증강 최고점 시기($p = 0.008$). MRI 점수체계는 곡선 하 면적이 0.972로 뛰어난 진단능을 나타내었고 이는 영상의학과 의사의 시각적 평가보다 유의미하게 높았다.

결론 MRI 점수체계는 황색육아종성 담낭염을 벽비후형 담낭암으로부터 감별진단하는 데 있어 영상의학과 의사의 시각적 평가보다 좋은 진단능을 나타내었다.

원광대학교병원 영상의학과